cold areas cross the wet mantle solidus curve (*21*) around a depth of ~100 km (Fig. 5B). Because of the characteristic kink on the solidus curve, the zone of partial melting is reached at approximately the same depth in all regions, provided volatiles are present. The thickness of the zone depends on the thermal state of the area. The base of the zone may be near the 400-km discontinuity in hot areas, whereas it is shallower in cold areas. We interpret the base of the partially molten zone as the Lehmann discontinuity; its depth is thus an indicator of the thermal state of the mantle.

The presence of a partially molten layer beneath continents at a relatively constant depth of ~100 km will affect the rheology of the mantle. Such a soft layer is a likely detachment for relative motion between plates. The viscosity of the layer is probably low, which may explain the apparent differences in thickness of the lithosphere as determined from seismological and rheological studies (*22*). One seismic profile, the N-striking Early Rise profile, does not reveal the 8° discontinuity. This is likely because the mantle below the central Canadian shield is cold, as indicated by the thick elastic lithosphere.

REFERENCES AND NOTES

1. A. Mohorovicic, *Jahrb. Meteorol. Obs. Zagreb* **9**, 1 (1909); H. Jeffreys, *Mon. Not. R. Astron. Soc. Geophys. Suppl*. **3**, 401 (1936); M. Niazi and D. L. Anderson, *J. Geophys. Res*. **70**, 4633 (1965).
2. I. Lehmann, *Ann. Geophys.* **15**, 93 (1959); _____, *Bull. Seismol. Soc. Am.* **54**, 123 (1964).
3. R. P. Masse, *Bull. Seismol. Soc. Am.* **63**, 911 (1973); S. K. Dey-Sarkar and R. A. Wiggins, *J. Geophys. Res.* **81**, 3619 (1976); K. Priestley, J. Cipar, A. Egorkin, N. Pavlenkova, *Geophys. J. Int.* **118**, 369 (1994); J. Mechie *et al.*, *Phys. Earth Planet. Inter*. **79**, 269 (1993).
4. P. M. Shearer, *Nature* **344**, 121 (1990).
5. S.-I. Karato, *Geophys. Res. Lett.* **19**, 2255 (1992); J. B. Gaherty and T. H. Jordan, *Science* **268**, 1468 (1995).
6. I. B. Lambert and P. J. Wyllie, *Nature* **219**, 1240 (1968); *Science* **169**, 764 (1970); A. L. Hales, *Geophys. J. Int.* **105**, 355 (1991).
7. J. Ansorge and St. Mueller, *Z. Geophys.* **39**, 385 (1973); K. Fuchs and L. P. Vinnik, *Geodyn. Ser. Am. Geophys. Union* **8**, 81 (1982).
8. A. Hirn *et al.*, *Z. Geophys.* **39**, 363 (1973).
9. E. Perchuć and H. Thybo, *Tectonophysics* **253**, 227 (1996).
10. C. Romney *et al.*, *Bull. Seismol. Soc. Am.* **52**, 1057 (1962).
11. BABEL Working Group, *Geophys. Res. Lett.* **18**, 645 (1991).
12. K. Fuchs and G. Müller, *Geophys. J. R. Astron. Soc.* **23**, 417 (1971).
13. F. Hauser, C. Prodehl, M. Schimmel, *Geophys. Inst. Open File Report 90-2* (University of Karlsruhe, Germany, 1990).
14. M. Walck, *Geophys. J. R. Astron. Soc.* **76**, 697 (1984).
15. H. J. van Heijst, R. Sneider, R. Nowack, *Geophys. J. Int.* **118**, 333 (1994).
16. A. M. Dziewonski and D. L. Anderson, *Phys. Earth Planet. Inter.* **25**, 297 (1981); B. L. N. Kennett and B. Engdahl, *Geophys. J. Int.* **105**, 429 (1991).
17. A. Zielhuis and G. Nolet, *Science* **265**, 79 (1994); J. Badal, V. Corchete, G. Payo, L. Pujades, J. A. Canas, *Geophys. J. Int.* **124**, 591 (1996); B. A. Romanovicz, *J. Geophys. Res.* **87**, 6865 (1982); R. Zeng, Z. Ding, Q. Wu, *Pure Appl. Geophys.* **145**, 423 (1995); L. J. Burdick, *J. Geophys. Res.* **86**, 5926 (1981); G. Poupinet *et al.*, *Tectonophysics*, in press.
18. K. Fuchs, *Tectonophysics* **56**, 1 (1983).
19. G. M. Mavko, *J. Geophys. Res.* **85**, 5173 (1980); H. Sato, I. S. Sacks, T. Murase, *ibid.* **94B**, 5689 (1989).
20. D. L. Anderson, in *Continental Mantle*, M. A. Menzies, Ed. (Oxford Science Publications, Oxford, 1990), pp. 1–30.
21. P. J. Wyllie, *J. Geophys. Res.* **85**, 6902 (1980); _____, *J. Geodyn.* **20**, 429 (1995).
22. T. M. Bechtel *et al.*, *Nature* **343**, 636 (1990); R. Hartley, A. B. Watts, J. D. Fairhead, *Earth Planet. Sci. Lett.* **137**, 1 (1996); K. Lambeck, P. Johnston, M. Nakada, *Geophys. J. Int.* **103**, 451 (1990).
23. J. Leliwa-Kopystynski and R. Teisseyre, Eds., *Constitution of the Earth's Interior* (PWN-Elsevier, Amsterdam, 1984), p. 171.
24. H. M. Iyer, L. C. Parkiser, D. J. Stuart, D. H. Warren, *J. Geophys. Res.* **74**, 4409 (1969); D. P. Hill, *Geol. Soc. Am. Bull.* **83**, 1639 (1972); J. W. Given and D. V. Helmberger, *J. Geophys. Res.* **85**, 7183 (1980); D. Mayer-Rosa and St. Mueller, *Z. Geophys.* **39**, 395 (1973); J. R. Bowman and B. L. N. Kennett, *Geophys. J. Int.* **101**, 411 (1990); S. Malone, personal communication; J. E. Vidale, X.-Y. Ding, S. P. Grand, *Geophys. Res. Lett.* **22**, 2557 (1995).

25. We thank A. Berthelsen (Copenhagen), F. Surlyk (Copenhagen), and P. J. Wyllie (Pasadena, CA) for comments to an earlier version of the manuscript. Supported by the Danish Natural Science Research Council and the Polish State Committee of Scientific Research.

11 October 1996; accepted 17 January 1997

Paleomagnetic Evidence of a Low-Temperature Origin of Carbonate in the Martian Meteorite ALH84001

Joseph L. Kirschvink, Altair T. Maine, Hojatollah Vali

Indirect evidence for life on Mars has been reported from the study of meteorite ALH84001. The formation temperature of the carbonates is controversial; some estimates suggest 20° to 80°C, whereas others exceed 650°C. Paleomagnetism can be used to distinguish between these possibilities because heating can remagnetize ferrimagnetic minerals. Study of two adjacent pyroxene grains from the crushed zone of ALH84001 shows that each possesses a stable natural remanent magnetization (NRM), implying that Mars had a substantial magnetic field when the grains cooled. However, NRM directions from these particles differ, implying that the meteorite has not been heated significantly since the formation of the internal crushed zone about 4 billion years ago. The carbonate globules postdate this brecciation, and thus formed at low temperatures.

McKay *et al.* (*1*) proposed that carbonate globules in the Antarctic meteorite ALH84001 may contain relict evidence of early life on Mars. This meteorite is an orthopyroxene cumulate (pyroxenite) that crystallized 4.5 billion years ago (Ga) (*2, 3*) and experienced shock metamorphism and formation of the internal crushed zone about 4.0 Ga (*4, 5*). It contains carbonate globules that apparently formed after this event (*6, 7*) but before the impact that presumably launched the sample from the surface of Mars approximately 15 million years ago (*8*). The interpretation (*1*) that these carbonates contain traces of ancient life requires that they formed at low temperatures, but their temperature of formation has been uncertain. An aqueous environment between 20° and 80° C is suggested by stable-isotope studies (*9*) and the co-occurrence of magnetite, iron monosulfides, and carbonate (*1*), whereas petrographic and electron microprobe results (*10, 11*) have been interpreted in support of carbonate formation temperatures of 650° to 700°C. Bradley *et al.* (*12*), for example, identified needle-like magnetite whiskers with occasional twins in the carbonate phase, and interpret them as high-temperature vapor phase deposits. However, needle-like magnetite crystals of similar size and shape are also produced biologically on Earth (*13*), as are twinned crystals (*14*).

Because magnetic minerals lock in the magnetic field direction when they cool below their critical blocking temperatures, paleomagnetism can be used to determine the thermal history of the ALH84001 meteorite (*15*). Rock-magnetic studies of other martian meteorites are consistent with the presence of a magnetic field on Mars of 1 to 10 μT in strength, at least as recently as 1.3 Ga (*16, 17*), and evidence from the Earth (*18*) and the moon (*19*) is consistent with the presence of a strong internal dynamo in the terrestrial planets early in their history. The Neél (~Curie) temperature of pure magnetite is 580°C, and the Neél temperatures of the pyrrhotite mineral family are

J. L. Kirschvink and A. T. Maine, Division of Geological and Planetary Sciences, California Institute of Technology, 170-25, Pasadena, CA 91125, USA.
H. Vali, Department of Earth and Planetary Sciences, McGill University, Montreal, Quebec H3A 2A7, Canada.

at or below ~325°C (*20*, *21*); blocking temperatures are lower for small grains.

We studied two pyroxene grains of ALH84001 (subsample 190) from its central crushed (breccia) zone (Fig. 1). The two grains are of unequal size and were joined at a fracture surface. Approximately 10 small carbonate globules like those described by McKay *et al.* (*1*), 50 to 200 μm in diameter with Fe-rich rims, are present on another flat fracture surface on the smaller grain (Fig. 1D). In addition, scanning electron microscope (SEM) analysis indicates that both pyroxene grains contain bright (SEM conductive) irregular inclusions that are 2 to 20 μm in size and rich in Fe and S (Fig. 1C). These inclusions are scattered irregularly over both broken and fractured surfaces of the pyroxene grains. Rare large chromite grains (which are paramagnetic) are also present (Fig. 1D). No pure Fe or Ti-oxides were detected outside of the carbonate globules. Of the Fe-S inclusions, only the pyrrhotite family ($Fe_{1-x}S$, where $0.13 \geq x \geq 0$) has ferrimagnetic states that could contribute to the magnetic remanence of the sample.

All sample manipulations were done on a laminar-flow (HEPA) clean bench housed in a class ~1000 dust-free, magnetically shielded clean lab facility (*22*). We developed several techniques specifically for this sample (*23*). After replicate measurements of the NRM vector, we separated the pyroxene grains along their approximate grain boundary with a diamond saw while preserving accurately their relative orientation (*24*). During two brief intervals where a thermal adhesive was applied or removed, the sample was heated to about 110°C. Because this was done in the ~300 nT residual magnetic field in the clean lab, this procedure should have demagnetized the low end of the blocking-temperature spectrum. We measured the NRM vectors of both pyroxene grains and recovered by vector subtraction the NRM vectors of the material removed by the sawing operation and that of a tiny chip of the small grain.

NRM vector directions measured from the large and small pyroxene grains differed by ~75° (Fig. 2 and Table 1). Although less well constrained, directions calculated for the material removed during the sawing operations lie reasonably close to the arc connecting these two pyroxene directions.

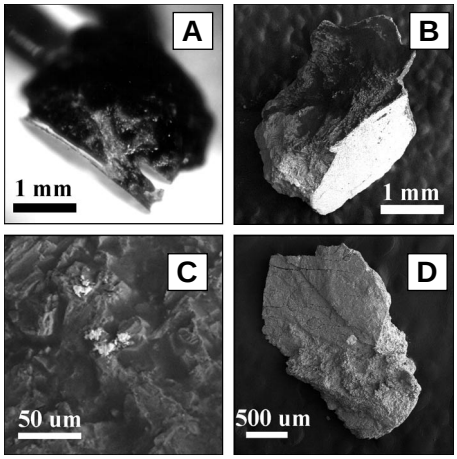

Fig. 1. Images of the sample of martian meteorite ALH84001. (**A**) Optical view of the intact sample mounted on a quartz-glass fiber, showing the first notch that was cut roughly along the boundary between the two pyroxene grains. The fiber holding the sample exits the image on the upper left margin. The flat surface on the lower left near the scale bar is the carbonate-bearing fracture surface [viewed face-on in (D)], covered with a thin layer of cyanoacrylate cement. The photograph was taken just after the Pyrex cover slip fell off during the first attempt at cutting. (**B**) SEM image of the large pyroxene grain. The bright-looking flat surface on the lower right is the plane of the saw cut. (**C**) SEM image of the surface of the large pyroxene grain. Elemental x-ray analysis indicates that the bright spots in the center are rich in Fe and S, which presumably contain the pyrrhotite responsible for holding the stable NRM of the sample. (**D**) SEM image of the fracture surface of the small pyroxene grain. Several of the carbonate-bearing globules are present on the fracture surface covering the top half of the grain. The bright spot near the center of the grain is a chromite grain, which should be paramagentic at room temperature.

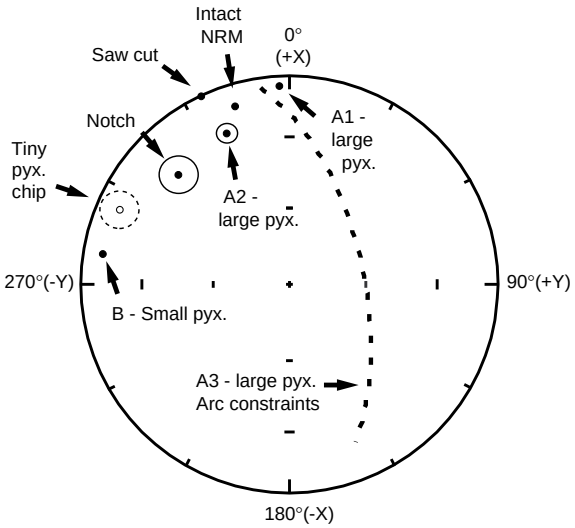

Fig. 2. Directions of the magnetic components isolated from a single 19.9-mg fragment from the central crushed zone of ALH84001, plotted on an equal-area stereonet. As the sample is unoriented, all directions are with respect to the right-handed Cartesian coordinate system of the magnetometer. Solid symbols are on the lower hemisphere (+*Z* values), whereas open symbols and dotted lines are upper hemisphere (−*Z* values). Error circles (1σ) are shown around points with errors of 5° or larger (as listed in Table 1). Labeled points are as follows: "Intact NRM" is the direction for the NRM of the sample before the sawing. Components A1-, A2-, and A3- were determined from the demagnetization analysis of the large pyroxene fragment; the long dotted line shows the arc-constraints, or locus of possible directions (*29*), for the as yet unresolved component A3. "B - Small pyx." is the univectoral component for the smaller oriented pyroxene grain containing the carbonate globules, and the direction of the small pyroxene chip broken off after the sawing cut is labeled "Tiny pyx. chip." The "Notch" and "Saw cut" points represent the directions held by materials removed by the sawing operations, as calculated by vector subtraction. Note that the "Notch" was centered on the grain boundary, whereas the "Saw cut" was adjusted to remove material mainly from the large pyroxene grain; this agrees with the location of their respective directions relative to components A1 and B.

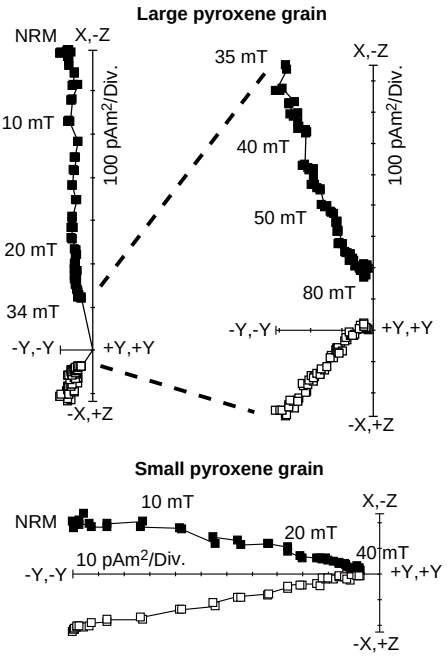

Fig. 3. Orthogonal projections of the vector demagnetization data for the oriented subsamples of the fragment of ALH84001. Solid symbols show projections of the vector on the X, Y plane (magnetometer coordinates), and open symbols show the Z, Y plane. The right-hand diagram for the large pyroxene grain is an enlargement of the data in the 35- to 80-mT interval. For the large pyroxene sample, the NRM remaining after each demagnetization step was measured thrice, whereas two measurements were made for the smaller grain.

Despite its larger error, the direction for the tiny chip is also close to the direction of its parent.

Although this large angular separation suggests that the NRM was acquired before brecciation of the rock, it is still necessary to check for the presence of a magnetically soft viscous remanent magnetization (VRM) that might have been acquired during the meteorite's 13,000-year (*25*) exposure to the Earth's magnetic field. A large VRM component in one of the grains could lead to the observed angular distance between their NRM vectors at room temperature. We performed two tests. First, we left the intact fragment of ALH84001 for 28 days in the low-field environment of the clean lab. Subsequent measurement revealed that there was no significant difference in direction or intensity. VRM components can usually be removed by a series of standard demagnetization experiments using three-axis alternating magnetic fields (AF demagnetization) of low intensity, generally <5-mT peak amplitude (*26*). Second, we put the oriented sub-samples through a series of progressively increasing AF demagnetization experiments, at peak intensities of up to 40 mT for both samples in increments of 1 or 2 mT, and up to 80 mT in steps of 2.5 and 5 mT for the larger pyroxene grain (*27*).

VRM components were not present in the low-field part of the coercivity spectra of either pyroxene grain. However, principal component analysis of the data (*28*) indicates that the large pyroxene grain had a multicomponent magnetization with at least three distinct, magnetically stable directions. The strongest of these was from the NRM to ~35 mT (component A1 in Table 1 and Fig. 2); this differed in direction by ~25° from the second direction (component A2), which was expressed from 40 to 80 mT. The presence of a third component with coercivities greater than 80 mT is indicated by the offset of the A2 line from the origin on Fig. 3. Arc-constraints on the demagnetization path (*29*) indicate that this direction must lie somewhere on the great circle arc labeled "A3" on Fig. 2. In contrast, the small pyroxene grain shows one basic component (termed "B") throughout its entire coercivity spectrum; this component differs in direction from the component of the large pyroxene grain A1 by ~77° and from component A2 by ~57°, and is farther still from the arc containing component A3.

A principal component deconvolution of the 0-40-mT AF demagnetization data for both oriented subsamples indicates that no component of the large pyroxene A1 direction is evident in the smaller sample, and vice versa; the directional components are present and clearly distinct above 5 mT (Fig. 4). Both spectra, however, have a similar shape; they peak at about 10 mT, and a tail extends up to 40 mT. This suggests that these components of the NRM are held by a similar suite of magnetic minerals. Comparison of the NRM magnetization levels, normalized for mass, indicates that the two components have similar intensities (4.5×10^{-5} and 5.6×10^{-5} Am^2/kg, for the large and small grains, respectively), well within the known range for thermoremanent magnetizations (TRM) from igneous rocks. The measured saturation isothermal remanent magnetization (IRM)/NRM ratios of 37 and 28 are also compatible with a TRM origin for these components. Although the Fe-S minerals in the pyroxene are apparently not magmatic (*30*), our data imply that they formed before final cooling and brecciation.

The large angular differences between the magnetic components isolated from the oriented pyroxene grains imply that the interior of the meteorite did not experience temperatures above the Neél point of the magnetic minerals during or after formation of the internal crushed zone. Because the carbonate globules were deposited on the fracture surfaces produced by this shock (*1*), this constraint must apply to them as well. This relative grain rotation is unlikely to have happened during the last shock event that launched the meteorite from Mars (*8*) because the rock would have fallen apart.

Better limits on the maximum temperature experienced by ALH84001 after brecciation can be placed with improved knowledge of the magnetic minerals holding the remanence in the two pyroxene grains. As shown in Fig. 5, most of the moment in the IRM curves for both grains was acquired in fields below 100 mT. This feature is similar for fine-grained dispersions of either magnetite or pyrrhotite. However, the IRM ac-

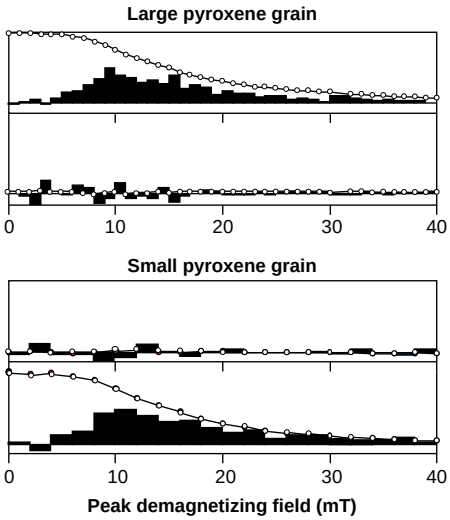

Fig. 4. Comparison of the coercivity spectra for components A1 and B, from the large and small pyroxene grains, respectively. This is a test for the presence of the large pyroxene A1 direction in the smaller grain, and vice versa. Demagnetization data were transformed from the orthogonal *X, Y, Z* Cartesian system of the magnetometer to a right-canted system using the normal direction vectors parallel to A1, B, and their cross-product (A1 × B). Normalized coefficients of components A1 and B are plotted as a function of the peak demagnetization field for both samples, and the histograms show the relative fraction removed between successive demagnetization steps. The vertical axis shows the scalar intensity of each component, normalized to the maximum moment for each sample. This deconvolution indicates that no consistent component of the large pyroxene grain's A1 direction is present within the smaller grain, and, similarly, no consistent component of direction (B) from the small pyroxene grain is present in the large grain. The coercivity spectra of components A1 and B overlap completely above the 5-mT level.

Table 1. Summary of NRM magnetic directions and principal magnetic components measured for a fragment of ALH84001 from the central crushed zone. Directions are given in polar coordinates, with declination values measured in degrees clockwise with respect to +*X*, and inclination values measured by the angle from the vector to the *X,Y* plane. Errors are expressed as the geometrical standard deviation (1σ maximum angular deviation, MAD), calculated with the least-squares technique of principal component analysis (*28*). Note that the intact sample weighed 19.9 mg; after the sawing operations the large pyroxene measured 12.7 mg, the small pyroxene fragment was 2.2 mg, and the tiny chip was 1.6 mg. This implies that 3.4 mg of the sample was lost in the two sawing operations.

NRM	Decl.	Incl.	Magnetic moment (10^{-12} Am^2)	Angular error (1σ)	Group
Intact NRM	342.9°	11.3°	1210	0.8°	6 point
Large pyroxene NRM	355.2°	8.8°	700	1.4°	3 point
Component A1	358.0°	5.6°	570	2.7°	91 point
Component A2	337.6°	22.9°	76	5.0°	61 point
Small pyroxene component B	279.3°	10.5°	123	2.2°	46 point
Notch NRM	318.7°	27.2°	102	10.6°	6-point derived
Saw cut NRM	334.9°	0.6°	312	1.3°	9-point derived
Tiny pyroxene chip	293.6°	−12.1°	40	9.1°	6-point derived

quisition curve for magnetite saturates (flattens) in fields greater than 300 mT (*20*), whereas that for pyrrhotite continues to acquire remanence up through applied fields greater than 1 Tesla (*31*). These data suggest, therefore, that pyrrhotite included in the pyroxene is the primary ferromagnetic mineral. Although the most abundant Fe-S phase in ALH84001 is pyrite (*10*), pyrrhotite also commonly occurs with pyrite (*21, 31*). However, the slope of the uppermost IRM acquisition curve of the small grain is noticeably shallower than that of the large pyroxene grain, suggesting that some magnetite may also be important.

Comparison of the AF demagnetization curves for the IRM and ARM also implies that pyrrhotite is the primary carrier of the NRM in the pyroxene grains (Fig. 5). In the large pyroxene grain, the ARM curve (solid symbols) falls well below that of the IRM demagnetization, suggesting that the particles are pseudo–single-domain grains or somewhat larger (*32*). This result is consistent with the SEM detection of fine-grained Fe-S inclusions in the pyroxene grains (Fig. 1C), and the known thermomagnetic properties of pyrrhotite (*20, 21*). For dispersions of strongly interacting single-domain magnetite, such as those present in the ALH84001 carbonate globules (*1*), the ARM demagnetization curve should lie well above that of the IRM (*33*). These ARM data from the small pyroxene grain (which has many of the carbonate globules) lie only slightly below those from the IRM demagnetization at values < 70 mT; above this, they switch positions. These data indicate that fine-grained magnetite in the small grain contributes to the rock magnetic properties. However, we do not know yet whether it contributes to the NRM.

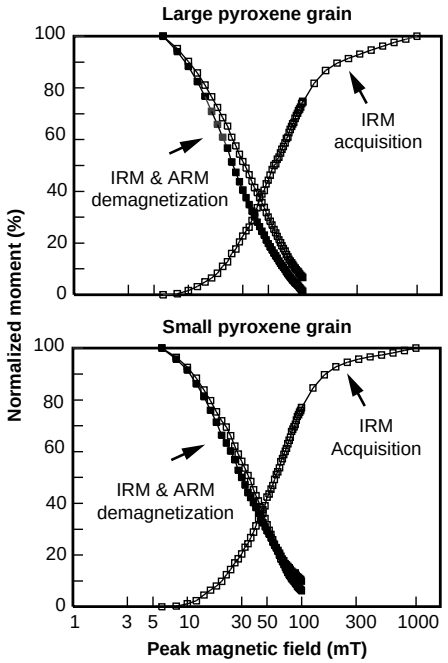

Fig. 5. Comparison of rock magnetic properties between the large and small pyroxene grains. The demagnetized samples were first given an anhysteretic remanent magnetization (ARM) by applying a 2-mT DC biasing field parallel to the sinusoidally oscillating (~800 Hz) alternating-field (AF) as it decayed from a peak amplitude of 100 mT. These ARMs were then AF demagnetized in progressively stronger fields (with zero biasing field) to generate the ARM demagnetization data shown (solid symbols). An isothermal remanent magnetization (IRM) was then given to the demagnetized samples using a ~1-ms, unidirectional pulse of 100 mT amplitude from a computer-controlled LC circuit, followed by progressive AF demagnetization to generate the IRM demagnetization data (open symbols). Finally, an IRM series with increasing peak fields up to 1 Tesla in strength produced the IRM acquisition data shown. As discussed in the text, these data are consistent with the NRM in the pyroxene being carried by fine-grained pyrrhotites, with a contribution from interacting, single-domain magnetite in the carbonate globules.

TRM intensities for natural pyrrhotites show almost a uniform decay of intensity with temperature up to the maximum Neél point of about 325 °C (*21*). This pattern implies that a thermal event even as short as a few seconds in duration should have left a detectable magnetic signal within the pyroxene grains down to ambient temperature. Because the blocking temperature of single-domain particles generally increases with coercive force (*20*), a component acquired in this fashion should at least have produced a nonlinear segment on the low-field end of the AF demagnetization diagrams (Fig. 3). Because components A1 and B are linear and distinct, the lowest thermal constraint these data can place on the post–4-billion-year thermal history of the ALH84001 internal crushed zone is set by the 110°C heating step used in applying the thermal adhesive in the sample preparation. Thermal demagnetization experiments of the intact NRM, conducted in an oxygen-free atmosphere, could clarify this interpretation.

These results support a model in which the pyroxenite of ALH84001 crystallized from an igneous melt at 4.5 Ga (*3*), and by 4 Ga had been exposed to at least one shock event, metamorphic heating, and chemical alteration (*4*), including formation of Fe-S inclusions in the pyroxene. All magnetic components probably formed during cooling in the martian magnetic field following this shock/metamorphic episode. The slight angular differences in the magnetic components (A3, A2, and A1) of the larger pyroxene grain could have formed either as a result of settling during cooling, or by shifts in the relative orientation of the martian magnetic field. Because of its small moment, we do not know whether the small pyroxene grain contains multiple magnetic components as does the larger particle. After cooling to ambient temperatures, brittle fracturing formed the internal crushed zone and rotated the grains. This also formed the fracture surfaces upon which the carbonate globules were later deposited, sometime in the interval 3.6 to 1.4 Ga (*6, 7*). From our data, we cannot say whether the magnetite and Fe-S minerals associated with the carbonate and found elsewhere on the fracture surfaces preserve a stable magnetic moment. However, Mars presumably had a magnetic field as late as 1.3 Ga (*16, 17*), which should have imparted some net alignment on these minerals as they formed. The impact ejection from Mars 15 million years ago (*8*), and passage through Earth's atmosphere 13,000 years ago (*25*), were both accomplished without significant heating of the meteorite's interior.

REFERENCES AND NOTES

1. D. McKay *et al.*, *Science* **273**, 924 (1996).
2. E. Jagoutz *et al.*, *Meteoritics* **29**, 478 (1994).
3. L. E. Nyquist, B. Bansal, H. Wiesmann, C.-Y. Shih, *Lunar Planet. Sci.* **XXVI**, 1065 (1995).
4. R. D. Ash, S. F. Knott, G. Turner, *Nature* **380**, 57 (1996).
5. A. H. Treiman, *Meteoritics* **30**, 294 (1995).
6. L. L. Griffith and E. L. Shock, *Nature* **377**, 406 (1995).
7. M. Wadhwa and G. W. Lugmair, *Meteoritics Planet. Sci.* **31** (suppl.), A145 (1996).
8. T. D. Swindle, J. A. Grier, M. K. Burkland, *Geochim. Cosmochim. Acta* **59**, 793 (1995).
9. C. S. Romanek *et al.*, *Nature* **372**, 655 (1994).
10. D. W. Mittlefehldt, *Meteoritics* **29**, 214 (1994).
11. R. P. Harvey and H. Y. Mcsween, *Nature* **382**, 49 (1996).
12. J. P. Bradley, R. P. Harvey, H. Y. McSween, *Geochim. Cosmochim. Acta* **60**, 5149 (1996).
13. H. Vali and J. L. Kirschvink, in *Iron Biomineralization*, R. P. Frankel and R. P. Blakemore, Eds. (Plenum, New York, 1991), pp. 97-115.
14. S. Mann *et al.*, *J. Exp. Biology* **140**, 35 (1988).
15. Several possibilities exist. First, if the crushed material in ALH84001 was heated either during or after carbonate precipitation, all of the pyroxene grains would be left magnetized in the same direction. Second, if the crushed zone cooled before the carbonates were precipitated, the pyroxene grains would have a uniform direction, but might differ from that of the carbonate. Third, if the crushed zone formed after the pyroxene had cooled, particles within it should have a dispersion of magnetic directions resulting from their physical rotation. This is a simple variation of the conglomerate test (*26*). Fourth, low to intermediate levels of heating after formation of the crushed zone should remagnetize only the lower portion of the blocking temperature spectrum of the meteorite, and the directionally consistent component could be recognized.
16. D. W. Collinson, *Earth Planet. Sci. Lett.* **7**, 159 (1986).
17. S. M. Cisowski, *Geochim. Cosmochim. Acta* **50**, 1043 (1986).
18. H. Tanaka *et al.*, *Geophys. J. Int.* **120**, 97 (1995).
19. S. K. Runcorn, *Geochim. Cosmochim. Acta* **60**, 1205 (1996).
20. W. O'Reilly, *Rock and Mineral Magnetism* (Blackie, London, 1984).
21. M. J. Dekkers, *Phys. Earth Planet. Inter.* **57**, 266 (1989). Note that K. L. Thomas *et al.* [*Lunar Planet. Sci.* **XXVII**, 1327 {1996}] have imaged inclusions of

magnetite within the pyroxene; however, these appear to have been formed on the fracture surfaces at the same time as the magnetite and Fe-sulfide phases associated with the carbonate globule.

22. J. L. Kirschvink, in *Biomagnetism: An Interdisciplinary Approach*, S. Williamson, Ed. (Plenum, New York, 1983), pp. 501-532.
23. The intact sample was mounted at one end of a quartz-glass fiber 15 cm long and 1 mm in diameter, which had been cleaned in concentrated HCl. It was attached to this fiber using cyanoacrylate cement that had been passed through a 0.2-μm syringe filter to remove ferromagnetic impurities (Fig. 1A). The opposite end of the fiber was attached to the vertex of a flat quartz-glass triangle, such that the open face of the carbonate layer on the fracture surface was aligned parallel to the triangle's surface. The edge of the triangle opposite from the fiber attachment was fused to an elongate hook, allowing the assembly to be suspended vertically on a thin (~200-g test) nylon fishing line U-loop. This loop was wound on a Teflon spool attached to a small computer-controlled stepping motor mounted on the ceiling of the clean-lab facility, and held directly above the room-temperature access port of the superconducting magnetometer. With this assembly, the sample could be raised and lowered smoothly from the sample loading position to a pair of computer-controlled solenoids for the demagnetization and rock magnetic experiments, and to the center of a three-axis superconducting moment magnetometer (a 2G Enterprises® model 570, with DC-biased SQuIDs). A horizontal arrow marked on the quartz triangle was aligned with the $+X$ direction of the superconducting moment magnetometer; vertical down was $+Z$, and the $+Y$ direction formed the third axis of a right-handed orthogonal coordinate system. We were able to obtain replicate measurements to better than 1% intensity, and 0.5° in direction, on magnetic moments as weak as 10^{-12} A m^{-2}, equivalent to the saturation remanence produced by ~20 picograms of single-domain (SD) magnetite.
24. This separation was done using a 150-μm-thick diamond-impregnated copper wafering saw. The flat surface of the carbonate-bearing grain was first glued to a thin Pyrex cover slip such that it was parallel to the surface of the quartz-glass triangle. The magnetic moment of this new assembly was indistinguishable from that measured prior to addition of the cover slip and the additional cement, confirming that they were both nonmagnetic. The other surface of the Pyrex cover slip was then bound to the surface of a cylindrical brass stub with a temperature-sensitive adhesive that had been filtered in acetone to remove ferromagnetic contaminants. The orientation of the quartz fiber was marked on the brass surface. Shortly after we began our first cut, the bond between the cyanoacrylic cement and the cover slip gave way. This left a small notch in the sample at the boundary between the pyroxene grains (Fig. 1A). By remeasuring the NRM of the sample after this step, we were able to calculate by difference the NRM vector that had been held by the material removed in the cut. Next, we fixed the flat surface of the carbonate-bearing layer directly to the brass stub with the adhesive, which held properly during the remainder of the wafering process. This last cut was adjusted slightly so that most material was removed from the larger grain, leaving a 2.2-mg fragment of the small pyroxene grain on the brass stub (Fig. 1D). While it was still bound to the stub, we then used the cyanoacrylate to cement a second quartz-glass triangle and fiber assembly to the this new fragment, with a relative orientation identical to that of the first sample. It was then freed from the brass stub by heating briefly to 110°C, and washed with filtered acetone to dissolve traces of the adhesive. The sawing procedure left a 1.6-mg fragment of the carbonate-bearing grain attached to the larger pyroxene grain. After measurement of the NRM, we were able to break this free with a nonmagnetic ceramic scalpel blade, and by remeasuring the NRM vector, were able to recover by difference the NRM vector of this small chip. The final weight of the pyroxene grain was 12.7 mg, implying that a total of 3.4 mg of the sample was lost in both sawing operations.
25. J. L. Gooding, *Icarus* **99**, 28 (1992).
26. R. F. Butler, *Paleomagnetism: Magnetic Domains to Geologic Terranes* (Blackwell, Boston, 1992).
27. AF demagnetization was not continued to higher levels for the small pyroxene grain because the intensity became weak and it had a linear decay toward the origin. Thermal demagnetization experiments were not done, because of the possibility of irreversible mineralogical changes on some of the Fe-S minerals, such as the iron monosulfides reported by McKay *et al*. (*1*).
28. J. L. Kirschvink, *Geophys. J. R. Astron. Soc.* **62**, 699 (1980).
29. P. L. Mcfadden and M. W. McElhinny, *Earth Planet. Sci. Lett.* **87**, 161 (1988).
30. C. K. Shearer *et al.*, *Geochim. Cosmochim. Acta* **60**, 2921 (1996).
31. M. J. Dekkers, *Phys. Earth Planet. Inter.* **52**, 376 (1988).
32. H. P. Johnson *et al.*, *Geophys. J. R. Astron. Soc.* **41**, 1 (1975).
33. S. Cisowski, *Phys. Earth Planet. Inter.* **26**, 56 (1981).
34. We thank D. McKay and E. K. Gibson for our sample of ALH84001, P. Carpenter for assistance with the SEM, and G. R. Rossman for help with the delicate sawing operation. H.V. acknowledges financial support from the U.S. National Research Council. We made extensive use of the software provided by C. Jones (cjones@mantle.colorado.edu) for the analysis and presentation of paleomagnetic data. B. C. Murray, J. Eiler, and D. A. Evans made helpful suggestions on the manuscript. This is contribution no. 5897 from the Division of Geological and Planetary Sciences of the California Institute of Technology.

31 January 1997; accepted 20 February 1997

Low-Temperature Carbonate Concretions in the Martian Meteorite ALH84001: Evidence from Stable Isotopes and Mineralogy

John W. Valley, John M. Eiler, Colin M. Graham, Everett K. Gibson, Christopher S. Romanek, Edward M. Stolper

The martian meteorite ALH84001 contains small, disk-shaped concretions of carbonate with concentric chemical and mineralogical zonation. Oxygen isotope compositions of these concretions, measured by ion microprobe, range from $\delta^{18}O = +9.5$ to $+20.5$‰. Most of the core of one concretion is homogeneous (16.7 ± 1.2‰) and over 5‰ higher in $\delta^{18}O$ than a second concretion. Orthopyroxene that hosts the secondary carbonates is isotopically homogeneous ($\delta^{18}O = 4.6 \pm 1.2$‰). Secondary SiO_2 has $\delta^{18}O = 20.4$‰. Carbon isotope ratios measured from the core of one concretion average $\delta^{13}C = 46 \pm 8$‰, consistent with formation on Mars. The isotopic variations and mineral compositions offer no evidence for high temperature (>650°C) carbonate precipitation and suggest non-equilibrium processes at low temperatures (<~300°C).

Carbonate concretions in ALH84001 provide information on the nature of the ancient martian atmosphere and hydrosphere, and aspects of their composition and morphology have been proposed as evidence for primitive life on Mars (*1*). The temperatures of carbonate formation are uncertain, but central to these questions. Mineral equilibria and the morphology of magnetite inclusions in carbonate have been used to infer temperatures of over 650°C (*2*, *3*), in which case carbon-based life is unlikely. On the other hand, oxygen isotope compositions of carbonate and the magnetic properties of millimeter-scale subdomains in ALH84001 have been interpreted to indicate that the minerals formed at temperatures of 0° to 110°C (*4*, *5*), suggesting precipitation during weathering or alteration. Such conditions would be permissive of life as we know it.

The ALH84001 meteorite is composed dominantly of igneous orthopyroxene ($Mg_{0.70}Fe_{0.27}Ca_{0.03}SiO_3$) with minor clinopyroxene, olivine, chromite, pyrite, apatite or whitlockite, maskelynite (shock-produced feldspathic glass $An_{31}Ab_{63}Or_6$), and SiO_2 (*2*, *6*, *7*). The sample is highly fractured, probably from impacts while it was still on Mars (*6*, *7*). Secondary carbonates are precipitated in some of these fractures and as disseminated patches in brecciated orthopyroxene (*2*, *6*, *7*).

We analyzed two carbonate concretions for isotopic and chemical compositions from a group of 14 that are approximately co-planar within an area of 2 mm^2 (Fig. 1A). Concretion #1 appears to be two concretions grown together, each of which has concentric core-to-rim chemical variations from $Ca_{0.15}Mg_{0.45}Fe_{0.40}CO_3$ to nearly pure $MgCO_3$ [Figs. 1C, 1D, 2, and figure 1 of

J. W. Valley, Department of Geology and Geophysics, University of Wisconsin, Madison, WI 53706, USA.
J. M. Eiler and E. M. Stolper, Division of Geological and Planetary Sciences, California Institute of Technology, Pasadena, CA 91125, USA.
C. M. Graham, Department of Geology and Geophysics, Edinburgh, EH9 3JW, Scotland, UK.
E. K. Gibson, NASA–Johnson Space Center, Houston, TX 77058, USA.
C. S. Romanek, Savannah River Ecology Laboratory, University of Georgia, Drawer E, Aiken, SC 29802, USA.